Edinburgh Research Explorer

An integrated pan-tropical biomass map using multiple reference datasets

OPEN ACCESS

1   **An integrated pan-tropical biomass map using multiple reference datasets**

2   (PAN-TROPICAL FUSED BIOMASS MAP)

3

4   Avitabile V. [1], Herold M. [1], Heuvelink G.B.M. [1], Lewis S.L. [2,3], Phillips O.L. [2], Asner G.P. [4],

5   Armston J. [5,6], Asthon P.[7,8], Banin L.F.[9], Bayol N. [10], Berry N.[11], Boeckx P.[12], de Jong B. [13],

6   DeVries B. [1], Girardin C. [14], Kearsley E. [12,15], Lindsell J.A. [16], Lopez-Gonzalez G. [2], Lucas R.

7   [17], Malhi Y. [14], Morel A. [14], Mitchard E. [11], Nagy L. [18], Qie L.[2], Quinones M. [19], Ryan C.M. [11],

8   Slik F. [20], Sunderland, T. [21], Vaglio Laurin G. [22], Valentini R. [23], Verbeeck H. [12], Wijaya A. [21],

9   Willcock S. [24]

10   1. Wageningen University, the Netherlands; 2. University of Leeds, UK; 3. University

11   College London, UK; 4. Carnegie Institution for Science, USA; 5. The University of

12   Queensland, Australia; 6. Information Technology and Innovation, Australia; 7. Harvard

13   University, UK; 8. Royal Botanic Gardens, UK; 9. Centre for Ecology and Hydrology, UK;

14   10. Foret Ressources Management, France; 11. University of Edinburgh, UK; 12. Ghent

15   University, Belgium; 13. Ecosur, Mexico; 14. University of Oxford, UK; 15. Royal Museum

16   for Central Africa, Belgium; 16. The RSPB Centre for Conservation Science, UK; 17. The

17   University of New South Wales, Australia; 18. Universidade Estadual de Campinas, Brazil;

18   19. SarVision, the Netherlands; 20. Universiti Brunei Darussalam, Brunei; 21. Center for

19   International Forestry Research, Indonesia; 22. Centro Euro-Mediterraneo sui Cambiamenti

20   Climatici, Italy; 23. Tuscia University, Italy; 24. University of Southampton, UK

21

22   Correspondence: Valerio Avitabile, tel. +31 317482092, email: valerio.avitabile@wur.nl

26 **Abstract**

27 We combined two existing datasets of vegetation aboveground biomass (AGB) (Saatchi et al.,

28 2011; Baccini et al., 2012) into a pan-tropical AGB map at 1-km resolution using an

29 independent reference dataset of field observations and locally-calibrated high-resolution

30 biomass maps, harmonized and upscaled to 14,477 1-km AGB estimates. Our data fusion

31 approach uses bias removal and weighted linear averaging that incorporates and spatializes

32 the biomass patterns indicated by the reference data. The method was applied independently

33 in areas (strata) with homogeneous error patterns of the input (Saatchi and Baccini) maps,

34 which were estimated from the reference data and additional covariates. Based on the fused

35 map, we estimated AGB stock for the tropics (23.4 N – 23.4 S) of 375 Pg dry mass, 9% - 18%

36 lower than the Saatchi and Baccini estimates. The fused map also showed differing spatial

37 patterns of AGB over large areas, with higher AGB density in the dense forest areas in the

38 Congo basin, Eastern Amazon and South-East Asia, and lower values in Central America and

39 in most dry vegetation areas of Africa than either of the input maps. The validation exercise,

40 based on 2,118 estimates from the reference dataset not used in the fusion process, showed

41 that the fused map had a RMSE 15 – 21% lower than that of the input maps and, most

42 importantly, nearly unbiased estimates (mean bias 5 Mg dry mass ha^{-1} vs. 21 and 28 Mg ha^{-1}

43 for the input maps). The fusion method can be applied at any scale including the policy-

44 relevant national level, where it can provide improved biomass estimates by integrating

45 existing regional biomass maps as input maps and additional, country-specific reference

46 datasets.

47

48

49   **Introduction**

50   Recently, considerable efforts have been made to better quantify the amounts and spatial

51   distribution of aboveground biomass (AGB), a key parameter for estimating carbon emissions

52   and removals due to land-use change, and related impacts on climate (Saatchi et al., 2011;

53   Baccini et al., 2012; Harris et al., 2012; Houghton et al., 2012; Mitchard et al., 2014; Achard

54   et al., 2014). Particular attention has been given to the tropical regions, where uncertainties

55   are higher (Pan et al., 2011; Ziegler et al., 2012; Grace et al., 2014). In addition to ground

56   observations acquired by research networks or for forest inventory purposes, several AGB

57   maps have been recently produced at different scales, using a variety of empirical modelling

58   approaches based on remote sensing data calibrated by field observations (e.g., Goetz et al.,

59   2011; Birdsey et al., 2013). AGB maps at moderate resolution have been produced for the

60   entire tropical belt by integrating various satellite observations (Saatchi et al., 2011; Baccini et

61   al., 2012), while higher resolution datasets have been produced at local or national level using

62   medium-high resolution satellite data (e.g., Avitabile et al., 2012; Cartus et al., 2014),

63   sometimes in combination with airborne Light Detection and Ranging (LiDAR) data (Asner

64   et al., 2012a, 2012b, 2013, 2014a). The various datasets often have different purposes:

65   research plots provide a detailed and accurate estimation of AGB (and other ecological

66   parameters or processes) at the local level, forest inventory networks use a sampling approach

67   to obtain statistics of biomass stocks (or growing stock volume) per forest type at the sub-

68   national or national level, while high-resolution biomass maps can provide detailed and

69   spatially explicit estimates of AGB density to assist natural resource management, and large

70   scale coarse-resolution datasets depict AGB distribution for global-scale carbon accounting

71   and modelling.

72

73   In the context of the United Nations mechanism for Reducing Emissions from Deforestation

74   and forest Degradation (REDD+), emission estimates obtained from spatially explicit biomass

75   datasets may be favoured over those based on mean values derived from plot networks. This

76   preference stems from the fact that plot networks are not designed to represent land cover

77   change events, which usually do not occur randomly and may affect forests with biomass

78   density systematically different from the mean value (Baccini and Asner, 2013). With very

79   few tropical countries having national AGB maps or reliable statistics on forest carbon stocks,

80   regional maps may provide advantages compared to the use of default mean values (e.g.,

81   IPCC (2006) Tier 1 values) to assess emissions from deforestation, as long as their accuracy is

82   reasonable and their estimates are not affected by systematic errors (Avitabile et al., 2011).

83   These conditions are difficult to assess, however, since rigorous validation of regional AGB

84   maps remains problematic, given their large area coverage and large mapping unit (Mitchard

85   et al., 2013), while ground observations are only available for a limited number of small

86   sample areas.

87

88   The comparison of two recent pan-tropical AGB maps (Saatchi et al., 2011; Baccini et al.,

89   2012) revealed substantial differences between the two products (Mitchard et al., 2013).

90   Further comparison with ground observations and high-resolution maps also highlighted

91   notable differences in AGB patterns at regional scales (Baccini and Asner, 2013; Hills et al.,

92   2013; Mitchard et al., 2014). Such comparisons have stimulated a debate over the use and

93   capabilities of different types of biomass products (Saatchi et al., 2014; Langner et al., 2014)

94   and have highlighted both the importance and sometimes the lack of integration of different

95   datasets. On one hand, the two pan-tropical maps are consistent in terms of methodology

96   because both use the same primary data source (GLAS LiDAR) alongside a similar modelling

97   approach to upscale the LiDAR data to larger scales. Moreover, they have the advantage of

98   being calibrated using hundreds of thousands of AGB estimates derived from height metrics

99   computed by a spaceborne LiDAR sensor distributed over the tropics. However, such maps

100   are based on remotely sensed variables that do not directly measure AGB, but are sensitive to

101   canopy cover and canopy height parameters that do not fully capture the AGB variability of

102   complex tropical forests. Furthermore, both products assume global or continental allometric

103   relationships in which AGB varies only with stand height, and further errors are introduced by

104   upscaling the calibration data to the coarser satellite data. On the other hand, ground plots use

105   allometric equations to estimate AGB at individual tree level using directly measurable

106   parameters such as diameter, height and species identity (hence wood density). However, they

107   have limited coverage, are not error-free, and compiling various datasets over large areas is

108   made more complex due to differing sampling strategies (e.g., stratification of landscapes,

109   plot size, minimum diameter of trees measured). Considering the rapid increase of biomass

110   observations at different scales and the different capabilities and limitations of the various

111   datasets, it is becoming more and more important to identify strategies that are capable of

112   making best use of existing information and optimally integrate various data sources for

113   improved large area AGB assessment (e.g., see Willcock et al., 2012).

114

115   In the present study, we compiled existing ground observations and locally-calibrated high-

116   resolution biomass maps to obtain a high-quality AGB reference dataset for the tropical

117   region (Objective 1). This reference dataset was used to assess two existing pan-tropical AGB

118   maps (Objective 2) and to combine them in a fused map that optimally integrates the two

119   maps, based on the method presented by Ge et al. (2014) (Objective 3). Lastly, the fused map

120   was assessed and compared to known AGB stocks and patterns across the tropics (Objective

121   4).

122

123   Overall, the approach consisted of pre-processing, screening and harmonizing the pan-tropical

124   AGB maps (called 'input maps'), the high-resolution AGB maps (called 'reference maps')

125   and the field plots (called 'reference plots'; 'reference dataset' refers to the maps and plots

126   combined) to a common spatial resolution and geospatial reference system (Figure 1). The

127   input maps were combined using bias removal and weighted linear averaging ('fusion'). The

128   fusion model was applied independently to areas associated with different error patterns of the

129   input maps (called 'error strata'), which were estimated from the reference data and additional

130   covariates (called 'covariate maps'). The reference dataset included only a subset of the

131   reference maps (i.e., the cells with highest confidence) and if a stratum was lacking reference

132   data ('reference data gaps'), additional data were extracted from the reference maps

133   ('consolidation'). The fused map was validated using independent data and its uncertainty

134   quantified using model parameters. In this study, the terms AGB refers to aboveground live

135   woody biomass and is reported in units of Mg dry mass ha^{-1}. The fused map and the

136   corresponding   reference   dataset   can   be   freely   downloaded   from

137   www.wageningenur.nl/grsbiomass.

138

139

140

141

142

143

144

145

146

147

148 **Materials and methods**

149 *Input maps*

150 The input maps used for this study were the two pan-tropical datasets published by Saatchi et

151 al. (2011) and Baccini et al. (2012), hereafter referred to as the "Saatchi" and "Baccini" maps

152 individually, or as "input" maps collectively. The Baccini map was provided in MODIS

153 sinusoidal projection with a spatial resolution of 463 m while the Saatchi map was in a

154 geographic projection (WGS-84) at 0.00833 degrees (approximately 1 km) pixel size. The

155 two datasets were harmonized by first projecting the Baccini map to the coordinate system of

156 the Saatchi map using the Geospatial Data Abstraction Library (www.gdal.org) and then

157 aggregating it to match the spatial resolution and grid of the Saatchi map. Spatial aggregation

158 was performed by computing the mean value of the pixels whose centre was located within

159 each 1-km cell of the Saatchi map. Resampling was then undertaken using the nearest

160 neighbor method.

161

162 *Reference dataset*

163 The reference dataset comprised individual tree-based field data and high-resolution AGB

164 maps independent from the input maps. The field data included AGB estimates derived from

165 field measurement of tree parameters and allometric equations. The AGB maps included high-

166 resolution ($\leq$ 100 m) datasets derived from satellite data using empirical models calibrated

167 and validated using local ground observations and, in some cases, airborne LiDAR

168 measurements. Given the variability of procedures used to acquire and produce the various

169 datasets, they were first screened according to a set of quality criteria to select only the most

170 reliable AGB estimates, and then pre-processed to be harmonized with the pan-tropical AGB

171 maps in terms of spatial resolution and observed variables. Field and map datasets providing

172 aboveground carbon density were converted to AGB units using the same coefficients used

173   for their original conversion from biomass to carbon. The sources and characteristics of the

174   reference data are listed in the Supplementary Information (Tables S8 - S11).

175

176   **Data screening and pre-processing**

177   *Reference field data*

178   The reference field data were measurements from forest inventory plots for which accurate

179   geolocation and biomass estimates were available. Pre-processing of the data consisted of a 2-

180   step screening and a harmonization procedure. A preliminary screening selected only the

181   ground data that satisfied the following criteria: (1) they estimated AGB for all living trees

182   with diameter at breast height $\geq$ 5-10 cm; (2) they were acquired on or after the year 2000; (3)

183   they were not used to calibrate the LiDAR-AGB relationships of the input maps; and (4) their

184   plot coordinates were measured using a GPS. Since the taxonomic identities of trees strongly

185   indicate wood density, and hence stand-level biomass (e.g., Baker et al., 2004; Mitchard et al.

186   2014), plots were only selected if tree AGB was estimated using at least tree diameter and

187   wood density as input parameters. Datasets were excluded if they did not conform to these

188   requirements or did not provide clear information on the biomass pool measured, the tree

189   parameters measured in the field, the allometric model applied, the year of measurement or

190   the plot geolocation and extent. Next, the plot data were projected to the geographic reference

191   system WGS-84 and harmonized with the input maps by averaging the AGB values located

192   within the same 1-km pixel if there was more than one plot per pixel, or by directly attributing

193   the plot AGB to the respective pixel if there was only one plot per pixel. Field plots not fully

194   located within one pixel were attributed to the map cell where the majority of the plot area

195   (i.e., the plot centroid) was located.

196

197   Lastly, the representativeness of the plot over the 1-km pixels was considered, and the ground

198   data were further screened to discard plots not representative of the map cells in terms of

199   AGB density. More specifically, since the two input maps in their native reference systems

200   are not aligned and therefore their pixels do not correspond to the same geographic area, the

201   plot representativeness was assessed on the area of both pixels (identified before the map

202   resampling). The representativeness was evaluated on the basis of the homogeneity of the tree

203   cover and crown size within the pixel, determined through visual interpretation of high-

204   resolution images provided on the Google Earth platform. If the tree cover and tree crowns

205   were not homogeneous over at least 90% of the pixel area, the plots located within the pixel

206   were discarded (Fig. S1). In addition, if subsequent Google Earth images indicated that forest

207   change processes (e.g., deforestation or regrowth) occurred in the period between the field

208   measurement and the reference years of the input maps, the corresponding plots were

209   discarded.

210

211   *Reference biomass maps*

212   The reference biomass maps consisted of high-resolution local or national AGB maps

213   published in the scientific literature. Maps providing AGB estimates grouped in classes (e.g.,

214   Willcock et al., 2012) were not used since the class values represent the mean AGB over large

215   areas, usually spanning multiple strata used in the present study (see 'Stratification approach').

216   The reference AGB maps were first pre-processed to match the input maps through re-

217   projection, aggregation and resampling using the same procedures described for the pre-

218   processing of the Baccini map. Then, only the cells with largest confidence (i.e., lowest

219   uncertainty) were selected from the maps. Since uncertainty maps were usually not available,

220   and considering that the reference maps were based on empirical models, the map cells with

221   greatest confidence were assumed to be those in correspondence of the training data (field

222   plots and/or LiDAR data). When the locations of the training data were not available, random

223   pixels were extracted from the maps. For maps based only on radar or optical data, whose

224   signals saturate above a certain AGB density value, only pixels below such a threshold were

225   considered. In order to compile a reference database that was representative of the area of

226   interest and well-balanced among the various input datasets (as defined in 'Consolidation of

227   the reference dataset'), the amount of reference data extracted from the AGB maps was

228   proportional to their area and not greater than the amount of samples provided by the field

229   datasets representing a similar area. In the case where maps with extensive training areas

230   provided a disproportionate number of reference pixels, a further screening selected only the

231   areas underpinned by the largest amount of training data.

232

233   **Consolidation of the reference dataset**

234   Considering that the modelling approach used in this study is applied independently by

235   stratum (which represent areas with homogeneous error structure in both input maps; see

236   'Stratification approach') and is sensitive to the characteristics of the reference data (see

237   'Modelling approach'), each stratum requires that calibration data are relatively well-balanced

238   between the various reference datasets. Specifically, if a stratum contains few calibration data,

239   the model becomes more sensitive to outliers, while if a reference dataset is much larger than

240   the others, the model is more strongly determined by the dominant dataset. For these reasons,

241   for the strata where the reference dataset was under-represented or un-balanced, it was

242   consolidated by additional reference data taken from the reference AGB maps, if available.

243   The reference data were considered insufficient if a stratum had less than half of the average

244   reference data per stratum, and were considered un-balanced if a single dataset provided more

245   than 75% of the reference data of the whole stratum and it was not representative of more than

246   75% of its area. In such cases, additional reference data were randomly extracted from the

247   reference AGB maps that did not provide more than 75% of the reference data. The amount of

248   data to be extracted from each map was computed in a way to obtain a reference dataset with

249   an average number of reference data per stratum and not dominated by a single dataset. If

250   necessary, additional training data representing areas with no AGB (e.g., bare soil) were

251   included, using visual analysis of Google Earth images to identify locations without

252   vegetation.

253

254   **Selected reference data**

255   The AGB reference dataset compiled for this study consisted of 14,477 1-km reference pixels,

256   distributed as follows: 953 in Africa, 449 in South America, 7,675 in Central America, 400 in

257   Asia and 5,000 in Australia (Fig. 2, Table 1). The reference data were relatively uniformly

258   distributed among the strata (Table S6) but their amount varied considerably by continent.

259   The average amount of reference data per stratum ranged from 50 (Asia) to 958 (Central

260   America) 1-km reference pixels and their variability (computed as standard deviation relative

261   to the mean) ranged from 25% (South America) to 52% (Central America). The uneven

262   distribution of reference data across the continents is mostly caused by the availability of

263   ground observations: as indicated above, in order to have a balanced reference dataset for

264   each stratum the reference data extracted from AGB maps were limited to the (smaller)

265   amount of direct field observations. When AGB maps were the only source of data, this

266   constraint was not occurring and larger datasets could be derived from the maps (i.e., Central

267   America, Australia).

268

269   The reference data were selected from 18 ground datasets and from 9 high-resolution AGB

270   maps calibrated by field observations and, in 4 cases, airborne LiDAR data (Table 1). The

271   field plots used for the calibration of the maps are not included in this section because they

272   were only used to select the reference pixels from the maps. The visual screening of the field

273   plots removed 35% of the input data (from 6,627 to 4,283) and their aggregation to 1-km

274   resolution further removed 70% of the reference units derived from field plots (from 4,283 to

275   1,274), while 10,741 reference pixels were extracted from the high-resolution AGB maps.

276   The criteria used to select the reference pixels for each map are reported in Table S2. The

277   consolidation procedure was necessary only for Central America where it added 2,415

278   reference data, while 47 pixels representing areas with no AGB were identified in Asia (Table

279   S1). In general, ground observations were mostly discarded in areas characterized by

280   fragmented or heterogeneous vegetation cover and high biomass spatial variability. In such

281   contexts, reference data were often acquired from the AGB maps.

282

283   ***Stratification approach***

284   Preliminary comparison of the reference data with the input maps showed that the error

285   variances and biases of the input maps were not spatially homogeneous but varied

286   considerably in different regions. Since the fusion model used in this study (see 'Modelling

287   approach') is based on bias removal and weighted combination of the input maps, the more

288   homogeneous the error characteristics in the input maps are, the better they can be reduced by

289   the model. For this reason, the stratification approach aimed at identifying areas with

290   homogeneous error structure (hereafter named 'error strata') in both input maps. A first

291   stratification was undertaken based on geographic location (namely Central America, South

292   America, Africa, Asia and Australia) to reflect the regional allometric relationships between

293   AGB and tree diameter and height (Feldpausch et al., 2011, 2012). Then, the error strata were

294   identified for each continent using a two-step process. First, the error maps of the Saatchi and

295   Baccini maps were predicted separately. Since the AGB estimates of the input maps were

296   mostly based on optical and LiDAR data that are sensitive to tree cover and tree height, it was

297   assumed that their uncertainties were related to the spatial variation of these parameters. In

298   addition, the errors of the input maps were found to be linearly correlated with the respective

299   AGB estimates. For these reasons, the AGB maps themselves, as well as global datasets of

300   land cover (ESA, 2014a), tree cover (Di Miceli et al., 2014) and tree height (Simard et al.,

301   2011), were used to predict the map errors using a Random Forest model (Breiman, 2001)

302   calibrated on the basis of the reference dataset. Second, the error maps of the Saatchi and

303   Baccini datasets were clustered using the K-Means approach. The use of eight clusters (hence,

304   eight error strata) was considered a sensible trade-off between homogeneity of the errors of

305   the input maps and number of reference observations available per stratum, with a larger

306   number of clusters providing only a marginal increase in homogeneity but leading to a small

307   number of reference data in some strata (Fig. S2). In areas where the predictors presented no

308   data (i.e., outside the coverage of the Baccini map) or for classes of the categorical predictor

309   without reference data (i.e., land cover), the error strata (instead of the error maps) were

310   predicted using an additional Random Forest model based on predictors without missing

311   values (i.e., Saatchi map, tree cover and tree height) and 10,000 training data randomly

312   extracted from the stratification map.

313

314   This method produced a stratification map that identified eight strata for each continent with

315   homogeneous error patterns in the input maps (Fig. S3). The root mean square error (RMSE)

316   computed on the Out-Of-Bag data (i.e., data not used for training) of the Random Forest

317   models that predicted the errors of the input maps ranged between 22.8 ± 0.3 Mg ha^{-1} (Central

318   America) to 83.7 ± 2.5 Mg ha^{-1} (Africa), with the two models (one for each input map)

319   achieving similar accuracies in each continent (Table S4, Fig. S4). In most cases the main

320   predictors of the errors of the input maps were the biomass values of the maps themselves,

321   followed by tree cover and tree height, while land cover was always the least important

322   predictor (Table S5). Further details on the processing of the input data are provided in the

323   Supplementary Information.

324

325   The use of a stratification based on the errors of the input maps was compared with

326   stratifications based on land cover (used by Ge et al., 2014), tree cover and tree height. A

327   separate stratification map was obtained for each of these alternative variables by aggregation

328   into eight strata (to maintain comparability with the number of clusters used in the error

329   strata), and each stratification map was used to develop a specific fused map. The

330   performance of alternative stratification approaches was assessed by validating the respective

331   fused maps (see Supplementary Information – Alternative stratification approaches). The

332   results demonstrated that the stratification based on error modelling and clustering (i.e., the

333   error strata) produced a fused map with higher accuracy than that of the maps based on other

334   stratification approaches, and therefore was used in this study (Fig. S5).

335

336   *Modelling approach*

337   **The fusion model**

338   The integration of the two input maps was performed with a fusion model based on the

339   concept presented by Ge et al. (2014) and further developed for this study. The fusion model

340   consists of bias removal and weighted linear averaging of the input maps to produce an output

341   with greater accuracy than each of the input maps. The reference AGB dataset described

342   above was used to calibrate the model and to assess the accuracy of the input and fused maps.

343   A specific model was developed for each stratum.

344

345   Following Ge et al. (2014), the *p* input maps for locations $s \in D$, where D is the geographical

346   domain of interest common to the input maps, were combined using a weighted linear average:

347　　　　　　　　　　(1) $f(s) = \sum_{i=1}^{p} w_i(s) \cdot (z_i(s) - v_i(s))$

348　　where f is the fused map, the $w_i(s)$ are weights, z_i the estimate of the i-th input map and $v_i(s)$ is

349　　the bias estimate. The bias term was computed as the average difference between the input

350　　map and the reference data for each stratum. The weights were obtained from a statistical

351　　model that assumes the map estimates z_i to be the sum of the true biomass b_i with a bias term

352　　v_i and a random noise term ε_i with zero mean for each location $s \in D$. We further assumed that

353　　the ε_i of the input maps are jointly normally distributed with variance-covariance matrix $\mathbf{C}(s)$.

354　　Differently from Ge et al. (2014), $\mathbf{C}(s)$ was estimated using a robust covariance estimator as

355　　implemented by the 'robust' package in R (Wang et al., 2014), which uses the Stahel-Donoho

356　　estimator for strata with fewer than 5,000 observations and the Fast Minimum Covariance

357　　Determinant estimator for larger strata. Under these assumptions, the variance of the

358　　estimation error of the fused map $f(s)$ is minimized by calculating the weights $w(s)$ as outlined

359　　by Searle (1971, p. 89):

360　　　　　　　　　(2) $w(s)^T = \left(\mathbf{1}^T \mathbf{C}(s)^{-1} \mathbf{1}\right)^{-1} \mathbf{1}^T \mathbf{C}(s)^{-1}$

361　　where $\mathbf{1} = [1, ..., 1]^T$ is the transpose of the p-dimensional unit vector. The weights computed

362　　for each stratum sum to 1, while their values are approximately inversely proportional to the

363　　error variance of the corresponding input map. Larger weights are assigned to input maps with

364　　lower error variances, although the covariance between map errors influences the weights as

365　　well. Overall, the fused map is expected to provide more accurate estimates after bias removal

366　　and weighted averaging of the input maps. The fusion model assured that the variance of the

367　　error in the fused map was smaller than that of the input maps (Bates and Granger, 1969),

368　　especially if the errors associated with these maps were not strongly positively correlated and

369　　their error variances were close to the smallest error variance. The fusion model can be

370　　applied to any number of input maps. Where there is only one input map, the model estimates

371　　and removes its bias and the weights are set equal to 1.

372

373 **The model parameters**

374 The fusion model computed a set of bias and weight parameters for each stratum and

375 continent on the basis of their respective reference data, and used these for the linear weighted

376 combination of the input maps (Table S6). Since the stratification approach grouped together

377 data with similar error patterns, the biases varied considerably among the strata and could

378 reach values up to ±200 Mg ha^{-1}. However, considering the area of the strata, the biases of

379 both input maps were smaller than ±45 Mg ha^{-1} for at least 50% of the area of all continents

380 and smaller than ±100 Mg ha^{-1} for 81% - 98% of the area of all continents.

381

382 *Post-processing*

383 **Predictions outside the coverage of the Baccini map**

384 The Baccini map covers the tropical belt between 23.4 degree north latitude and 23.4 degree

385 south latitude while the Saatchi map presents a larger latitudinal coverage (Fig. 2). The fusion

386 model was first applied to the area common to both input maps (Baccini extent) and then

387 extended to the area where only the Saatchi map is available. In the latter area, the model

388 focused only on removing the bias of the Saatchi map using the values estimated for the

389 Baccini extent. The model predictions for the Saatchi extent were mosaicked to those for the

390 Baccini extent using a smoothing function (inverse distance weight) on an overlapping area of

391 1 degree within the Baccini extent between the two maps. Water bodies were masked over the

392 whole study area using the ESA CCI Water Bodies map (ESA, 2014b). The resulting fused

393 map was projected to an equal area reference system (MODIS Sinusoidal) before computing

394 the total AGB stocks for each continent, which were obtained by summing the products of the

395 AGB density of each pixel with their area.

396

397 **Assessing AGB in intact and non-intact forest**

398 The AGB estimates of the fused and input maps in forest areas were further investigated

399 regarding their distribution in ecozones and between intact and non-intact landscapes. Forest

400 areas were defined as areas dominated by tree cover according to the GLC2000 map

401 (Bartholomé and Belward, 2005). Ecozones were defined according to the Global Ecological

402 Zone (GEZ) map for the year 2000 (FAO, 2000). The intact landscapes were defined

403 according to the Intact Forest Landscape (IFL) map for the year 2000 (Potapov et al., 2008).

404 On the basis of these datasets, the mean forest AGB density of the fused and input maps were

405 computed for intact and non-intact landscapes for each continent and major ecozone. To allow

406 direct comparison of the results among the maps, the analysis was performed only for the area

407 common to all maps (Baccini extent). In addition, to reduce the impact of spatial inaccuracies

408 in the maps, only ecozones with IFL intact forest areas larger than 1,000 km^2 were considered.

409 The mean AGB density of intact and non-intact forests per continent was computed as the

410 area-weighted mean of the contributing ecozones.

411

412 *Validation and uncertainty*

413 Validation of the fused and input maps was performed by randomly splitting the reference

414 data into a calibration set (70% of the data) and a validation set (remaining 30%). The 'final'

415 fused map presented in Fig. 3 used 100% of the reference data while for validation purposes a

416 'test' fused map was produced using only the calibration data. The estimates of the 'test'

417 fused map, as well as those of the input maps, were compared with the validation data. Note

418 that validation of the 'test' fused map only yields an approximate (i.e., conservative) estimate

419 of the accuracy of the 'final' fused map. In other words, the 'final' fused map is likely more

420 accurate than the 'test' fused map because it uses a larger calibration data set. To maintain full

421 independence, validation data were not used for any step related to the development of the

422   'test' fused map, including production of the stratification map. To account for any potential

423   impacts of the random selection of validation data, the procedure was repeated 100 times,

424   computing a new random selection of the calibration and validation datasets with each

425   iteration. This procedure allowed computing the mean RMSE and assessing its standard

426   deviation for the fused and input maps.

427

428   The uncertainty of the fused map was computed with respect to model uncertainty, not

429   including the error sources in the input data (see 'Discussion'). The model uncertainty

430   consisted of the expected variance of the error of the fused map (which is assumed to be bias-

431   free) and was derived for each stratum from $C_{(s)}$. The uncertainty was thus estimated per

432   strata and not at the pixel level. The error variance was converted to an uncertainty map by

433   reclassifying the stratification map, where the stratum value was converted to the respective

434   error variance computed for each stratum and continent.

435

436

437

438

439

440

441

442

443

444

445

446

447   **Results**

448   *Biomass map*

449   The fusion model produced an AGB map at 1-km resolution for the tropical region, with an

450   extent equal to that of the Saatchi map (Fig. 3). In terms of stocks, the AGB estimates within

451   the fused map were lower than both input maps at continental level. The total stock of the

452   fused map for the tropical belt covered by the Baccini map (23.4 N – 23.4 S, see Fig. 2) was

453   375 Pg dry mass, 9% and 18% lower than the Saatchi (413 Pg) and Baccini (457 Pg)

454   estimates, respectively. Considering the larger extent of the Saatchi map, the fused map

455   estimate was 462 Pg, 15% lower than the estimate of the Saatchi map (545 Pg) (Table S7).

456

457   Moreover, the fused map presented spatial patterns that differed substantially from both input

458   maps (Fig. 4): the AGB estimates were higher than the Saatchi and Baccini maps in the dense

459   forest areas in the Congo basin, in West Africa, in the north-eastern part of the Amazon basin

460   (Guyana shield) and in South-East Asia, and lower in Central America and in most dry

461   vegetation areas of Africa. In the central part of the Amazon basin the fused map showed

462   lower estimates than the Baccini map and higher estimates than the Saatchi map, while in the

463   southern part of the Amazon basin these differences were inversed. Similar trends emerged

464   when comparing the maps separately for intact and non-intact forest ecozones (Supporting

465   Information). In addition, the average difference between intact and non-intact forests was

466   larger than that derived from the input maps in Africa and Asia, similar or slightly larger in

467   South America, and smaller in Central America (Fig. S6).

468

469   According to the fused map, the highest AGB density (> 400 Mg ha^{-1}) is found in the Guyana

470   shield, in the central and western part of the Congo basin and in the intact forest areas of

471   Borneo and Papua New Guinea. The analysis of the distribution of forest AGB in intact and

472   non-intact ecozones showed that the mean AGB density was greatest in intact African (360

473   Mg ha^{-1}) and Asian (335 Mg ha^{-1}) forests, followed by intact forests in South America (266

474   Mg ha^{-1}) and Central America (146 Mg ha^{-1}) (Fig. S6). AGB in non-intact forests was much

475   lower in all regions (Africa, 78 Mg ha^{-1}; Asia, 211 Mg ha^{-1}; South America, 149 Mg ha^{-1}; and

476   Central America, 57 Mg ha^{-1}) (Fig. S6).

477

478   *Validation*

479   The validation exercise showed that the fused map achieved a lower RMSE (a decrease of 5 –

480   74%) and bias (a decrease of 90 – 153%) than the input maps for all continents (Fig. 5). While

481   the RMSE of the fused map was consistently lower than that of the input maps but still

482   substantial (87 – 98 Mg ha^{-1}) in the largest continents (Africa, South America and Asia), the

483   mean error (bias) of the fused map was almost null in most cases. Moreover, in the three main

484   continents the bias of the input maps tended to vary with biomass, with overestimation at low

485   values and underestimation at high values, while the errors of the fused map were more

486   consistently distributed (Fig. 6). When computing the error statistics for the pan-tropics

487   (Baccini extent) as the average of the regional validation results weighted by the respective

488   area coverage, the mean bias (in absolute terms) for the fused, Saatchi and Baccini maps was

489   5, 21 and 28 Mg ha^{-1} and the mean RMSE was 89, 104 and 112 Mg ha^{-1}, respectively (Fig. 5).

490   The accuracy of the input maps reported above was computed using the validation dataset

491   (30% of the reference dataset) to be consistent with the accuracy of the fused map. The

492   accuracy of the input maps was also computed using all reference data and the results (Table

493   S3) were similar to those based on the validation dataset.

494

495   *Uncertainty map*

496   The uncertainty of the model predictions indicated that the standard deviation of the error of

497   the fused map for each stratum was in the range 11 - 108 Mg ha^{-1}, with largest uncertainties in

498   areas with largest AGB estimates (Congo basin, Eastern Amazon basin and Borneo). When

499   computed in relative terms (as a percentage of the AGB estimate), the model uncertainties

500   presented opposite patterns, with uncertainties larger than the estimates (> 100%) in the low

501   AGB areas (< 20 Mg ha^{-1} on average) of Africa, South America and Central America, while

502   high AGB forests (> 210 Mg ha^{-1} on average) had uncertainties lower than 25% (Fig. 7). The

503   uncertainty measure derived from *C(s)* was computed only when two or more input maps

504   were available. Hence, it could not be calculated for Australia because the model for this

505   continent was based on only one input map (Saatchi map).

506

507

508

509

510

511

512

513

514

515

516

517

518

519

520 **Discussion**

521 *Biomass patterns and stocks emerging from the reference data*

522 The AGB map produced with the fusion approach is largely driven by the reference dataset

523 and essentially the method is aimed at spatializing the AGB patterns indicated by the

524 reference data using the support of the input maps. For this reason, great care was taken in the

525 pre-processing of the reference data, which included a two-step quality screening based on

526 metadata analysis and visual interpretation, and their consolidation after stratification. As a

527 result, the reference dataset provides an unprecedented compilation of AGB estimates at 1-km

528 resolution for the tropical region, covering a wide range of vegetation types, biomass ranges

529 and ecological regions across the tropics. It includes the most comprehensive and accurate

530 tropical field plot networks and high-quality maps calibrated with airborne LiDAR, which

531 provide more accurate estimates compared to those obtained from other sensors (Zolkos et al.,

532 2013). The main trends present in the fused map emerged from the combination of different

533 and independent reference datasets and are in agreement with the estimates derived from

534 long-term research plot networks (Malhi et al., 2006; Phillips et al., 2009; Lewis et al., 2009;

535 Slik et al., 2010, 2013; Lewis et al., 2013) and high-resolution maps (Asner et al., 2012a,

536 2012b, 2013, 2014a). Specifically, the AGB patterns in South America represent spatial

537 trends described by research plot networks in the dense intact and non-intact forests in the

538 Amazon basin, forest inventory plots collected in the dense forests of Guyana and samples

539 extracted from AGB maps for Colombia and Peru representing a wide range of vegetation

540 types, from arid grasslands to humid forests. Similarly, AGB patterns depicted in Africa were

541 derived from a combination of various research plots in dense undisturbed forest (Gabon,

542 Cameroon, Democratic Republic of Congo, Ghana, Liberia), inventory plots in forest

543 concessions (Democratic Republic of Congo), AGB maps in woodland and savannah

544 ecosystems (Uganda, Mozambique) and research plots and maps in montane forests (Ethiopia,

545   Madagascar). Most vegetation types in Central America, Asia and Australia were also well-

546   represented by the extensive forest inventory plots (Indonesia, Vietnam and Laos) and high-

547   resolution maps (Mexico, Panama, Australia).

548

549   In spite of the extensive coverage, the current database is far from being representative of the

550   AGB variability across the tropics. As a consequence, the model estimates are expected to be

551   less accurate in contexts not adequately represented. In the case of the fusion approach, this

552   corresponds to the areas where the input maps present error patterns different than those

553   identified in areas with reference data: in such areas the model parameters used to correct the

554   input maps (bias and weight) may not adequately reflect the errors of the input maps and

555   hence cannot optimally correct them. In particular, deciduous vegetation and heavily

556   disturbed forest of Africa and South America, and large parts of Asia were lacking quality

557   reference data. Moreover, even though plot data were spatially distributed over the central

558   Amazon and the Congo basin, large extents of these two main blocks of tropical forest have

559   never been measured (cf. maps in Lewis et al., 2013; Mitchard et al., 2014). Considering the

560   evidence of significant local differences in forest structure and AGB density within the same

561   forest ecosystems (Kearsley et al., 2013), additional data are needed to strengthen the

562   confidence of the fused map as well as that of any other AGB map covering the tropical

563   region. Moreover, a dedicated gap analysis to assess the main regions lacking AGB reference

564   data and identify priority areas for new field sampling and LiDAR campaigns would be very

565   valuable for future improved biomass mapping.

566

567   Regarding the AGB stocks, a previous study showed that despite their often very strong local

568   differences, the two input maps tended to provide similar estimates of total stocks at national

569   and biome scales and presented an overall net difference of 10% for the pan-tropics (Mitchard

570 et al., 2013). However, such convergence is mostly due to compensation of contrasting

571 estimates when averaging over large areas. The larger differences with the estimates of the

572 present study (9% and 18%) suggest an overestimation of the total stocks by the input maps.

573 This is in agreement with the results of two previous studies that, on the basis of reference

574 maps obtained by field-calibrated airborne LiDAR data, identified an overestimation of 23% -

575 42% of total stocks in the Saatchi and Baccini maps in the Colombian Amazon (Mitchard et

576 al., 2013) and a mean overestimation of about 100 Mg ha^{-1} for the Baccini map in the

577 Colombian and Peruvian Amazon (Baccini and Asner, 2013).

578

579 In general, the AGB density values of the fused map were calibrated and therefore in

580 agreement with the existing estimates obtained from plot networks and high-resolution maps.

581 The comparison of mean AGB values in intact and non-intact forests stratified by ecozone

582 provided further information on the differences between the maps. The mean AGB values of

583 the fused map in non-intact forests were mostly lower than those of the input maps,

584 suggesting that in disturbed forests the AGB estimates derived from stand height parameters

585 retrieved by spaceborne LiDAR (as in the input maps) tend to be higher compared to those

586 based on tree parameters or very high-resolution airborne LiDAR measurements (as in the

587 fused map and reference data). This difference occurred especially in Africa, Asia and Central

588 America while it was less evident in South America and Australia. By contrast, the

589 differences among the maps for intact forests varied by continent, with the fused map having,

590 on average, higher mean AGB values in Africa, Asia and Australia, lower values in Central

591 America, and variable trends within South America, reflecting the different allometric

592 relationships used by the various datasets in different continents.

593

594　　As mentioned above, a larger amount of reference data, ideally acquired based on a clear

595　　statistical sampling design instead of one that is opportunistic, will be required to confirm

596　　such conclusions. While dense sampling of tropical forests using field observations is often

597　　impractical, new approaches combining sufficient ground observations of individual trees at

598　　calibration plots with airborne LiDAR measurements for larger sampling transects would

599　　allow a major increase in the quantity of calibration data. In combination with wall-to-wall

600　　medium resolution satellite data (e.g., Landsat) these may be capable of achieving high

601　　accuracy over large areas (10% - 20% uncertainty at 1-ha scale) while being cost-effective

602　　(e.g., Asner et al., 2013, 2014b). In addition, new technologies, such as Terrestrial Laser

603　　Scanning (TLS), allows for better estimates at ground level (Calders et al., 2015; Gonzalez de

604　　Tanago et al., 2015), considerably reducing the uncertainties of field estimates based on

605　　generalized allometric equations and avoiding destructive sampling. Nevertheless, since

606　　floristic composition influences AGB at multiple scales (e.g., the strong pan-Amazon gradient

607　　in wood density shown by ter Steege et al., 2006) such techniques benefit from extensive and

608　　precise measurements of tree identity in order to determine wood density patterns and to

609　　account for variations in hollow stems and rottenness (Nogueira et al., 2006). Moreover, we

610　　note that the reference data do not include lianas, which may constitute a substantial amount

611　　of woody stems, and their inclusion would allow to obtain more correct estimates of total

612　　AGB of vegetation (Phillips et al., 2002; Schnitzer & Bongers, 2011; Durán & Gianoli, 2013).

613

614　　***Additional error sources***

615　　Apart from the uncertainty of the fusion model described above (see 'Uncertainty'), three

616　　other sources of error were identified and assessed in the present approach: i) errors in the

617　　reference dataset; ii) errors due to temporal mismatch between the reference data and the

618　　input maps; iii) errors in the stratification map.

619

620   **Errors in the reference dataset**

621   The reference dataset is not error-free but it inherits the errors present in the field data and

622   local maps. In addition, additional uncertainties are introduced during the pre-processing of

623   the data by resampling the maps and upscaling the plot data to 1-km resolution. In particular,

624   while the geolocation error of the original datasets was considered relatively small (< 50 m)

625   since plot coordinates were collected using GPS measurements and the AGB maps were

626   based on satellite data with accurate geolocation (i.e., Landsat, ALOS, MODIS), larger errors

627   (up to 500 m, half a pixel) could have been introduced with the resampling of the 1-km input

628   maps. All these error sources were minimized by selecting only the datasets that fulfilled

629   certain quality criteria and by further screening them through visual analysis of high-

630   resolution images available on the Google Earth platform, discarding the data not

631   representative of the respective map pixels. In case of reference data that clearly did not

632   match with the high-resolution images and/or with the input maps (e.g., reporting no AGB in

633   dense forest areas or high AGB on bare land), the data were considered as an error in the

634   reference dataset, a geolocation error in the plots or maps, or it was assumed that a land

635   change process occurred between the plot measurement and the image acquisition time (see

636   next paragraph).

637

638   **Errors due to temporal mismatch**

639   The temporal difference of input and reference data introduced some uncertainty in the fusion

640   model. The input maps refer to the years 2000 – 2001 (Saatchi) and 2007 – 2008 (Baccini)

641   while the reference data mostly spanned the period 2000 – 2013. Therefore, the differences

642   between the input maps and the reference data may also be due to a temporal mismatch of the

643   datasets. However, changes due to deforestation were most likely excluded during the visual

644   selection of the reference data, when high-resolution images showed clear land changes (e.g.,

645   bare land or agriculture) in areas where the input maps provided AGB estimates relative to

646   forest areas (or *vice-versa*, depending on the timing of acquisition of the datasets). However,

647   changes due to forest regrowth and degradation events that did not affect the forest canopy

648   could not be considered with the visual analysis and may have affected the mismatch

649   observed between the reference data and the input maps ($< 58 – 80$ Mg ha^{-1} for 50% of the

650   cases of the Saatchi and Baccini maps, respectively). Part of the mismatch was in the range of

651   AGB changes that can be attributes to regrowth ($1 – 13$ Mg ha^{-1} year^{-1}) (IPCC, 2003) or low-

652   intensity degradation ($14 – 100$ Mg ha^{-1}, or $3 – 15\%$ of total stock) (Asner et al., 2010;

653   Pearson et al., 2014). On the other hand, considering the limited area affected by degradation

654   (about 20% in the humid tropics) (Asner et al., 2009), the temporal mismatch could be

655   responsible only for a correspondent part of the differences observed between the reference

656   data and the input maps. Small additional offsets may also be caused by the documented

657   secular changes in AGB density within intact tropical forests, which has been increasing by

658    $0.2 – 0.5\%$ per year (Phillips et al., 1998, Chave et al., 2008, Phillips and Lewis, 2014). It

659   should also be noted that the reference data were used to optimally integrate the input maps,

660   and in the case of a temporal difference the fused map was 'actualized' to the state of the

661   vegetation when the reference data were acquired. The reference data were acquired between

662   2000 and 2013, and their mean acquisition year weighted by their contribution to the fusion

663   model (by continent) corresponds to the period $2007 – 2010$ (2007 in Africa, 2008 in Central

664   America, 2009 in South America and 2010 in Asia). Therefore the complete fused map cannot

665   be attributed to a specific year and more generally it represents the first decade of the 2000s.

666

667   **Errors in the stratification map**

668   The errors in the stratification map (i.e., related to the prediction of the errors of the input

669   maps) were still substantial in some areas and affected the fused map in two ways. First, the

670   reference data that were erroneously attributed to a certain stratum introduced 'noise' in the

671   estimation of the model parameters (bias and weight), but the impact of these 'outliers' was

672   largely reduced by the use of a robust covariance estimator. Second, erroneous predictions of

673   the strata caused the use of incorrect model parameters in the combination of the input maps.

674   The latter is considered to be the main source of error of the fused map and indicates that the

675   method can achieve improved results if the errors of the input maps can be predicted more

676   accurately. However, additional analysis showed that, on average, fused maps based on

677   alternative stratification approaches achieved lower accuracy than the map based on an error

678   stratification approach (Fig. S5). Therefore, this approach was preferred over a stratification

679   based on an individual biophysical variable (e.g., tree cover, tree height, land cover or

680   ecozone).

681

682   *Application of the method at national scale*

683   The fusion method presented in this study allows for the optimal integration of any number of

684   input maps to match the patterns indicated by the reference data. However, the accuracy of the

685   fused map depends on the availability of reference data representative of the error patterns of

686   the input maps. While the current reference database does not represent adequately all error

687   strata for the tropical region, and the model estimates are expected to have lower confidence

688   in under-represented areas, the proposed method may be applied locally and provide

689   improved AGB estimates where additional reference data are available. For example, the

690   fusion method may be applied at national level using existing forest inventory data, research

691   plots and local maps that cover only part of the country to calibrate global or regional maps,

692   which provide national coverage but may not be tailored to the country context. Such country-

693   calibrated AGB maps may be used to support natural resource management and national

694   reporting under the REDD+ mechanism, especially for countries that have limited capacities

695   to map AGB from remote sensing data (Romijn et al., 2012). Considering the increasing

696   number of global or regional AGB datasets based on different data and methodologies

697   expected in the coming years, and that likely there will not be a single 'best map' but rather

698   the accuracy of each will vary spatially, the fusion approach may allow to optimally combine

699   and adjust available datasets to local AGB patterns identified by reference data.

700

701

702

703

704

705

706

707

708

709

710

711

712

713

714

715

716

717

Acknowledgments

References

743   **References**

744   Achard F, Beuchle R, Mayaux P et al. (2014) Determination of tropical deforestation rates

745   and related carbon losses from 1990 to 2010. *Global Change Biology*, **20**, 2540–2554.

746   Asner GP, Clark JK, Mascaro J et al. (2012a) High-resolution mapping of forest carbon stocks

747   in the Colombian Amazon. *Biogeosciences*, **9**, 2683–2696.

748   Asner GP, Clark JK, Mascaro J et al. (2012b) Human and environmental controls over

749   aboveground carbon storage in Madagascar. *Carbon Balance and Management*, **7**, 2.

750   Asner GP, Mascaro J, Anderson C et al. (2013) High-fidelity national carbon mapping for

751   resource management and REDD+. *Carbon balance and management*, **8**, 7.

752   Asner GP, Knapp DE, Martin RE et al. (2014a) Targeted carbon conservation at national

753   scales with high-resolution monitoring. *Proceedings of the National Academy of*

754   *Sciences*, **111**, E5016–E5022.

755   Asner GP, Mascaro J (2014b) Mapping tropical forest carbon: Calibrating plot estimates to a

756   simple LiDAR metric. *Remote Sensing of Environment*, **140**, 614–624.

757   Avitabile V, Herold M, Henry M, Schmullius C (2011) Mapping biomass with remote

758   sensing: a comparison of methods for the case study of Uganda. *Carbon Balance and*

759   *Management*, **6**, 7.

760   Avitabile V, Baccini A, Friedl MA, Schmullius C (2012) Capabilities and limitations of

761   Landsat and land cover data for aboveground woody biomass estimation of Uganda.

762   *Remote Sensing of Environment*, **117**, 366–380.

763   Baccini A, Goetz SJ, Walker WS et al. (2012) Estimated carbon dioxide emissions from

764   tropical deforestation improved by carbon-density maps. *Nature Climate Change*, **2**,

765   182–185.

766   Baccini A, Asner GP (2013) Improving pantropical forest carbon maps with airborne LiDAR

767   sampling. *Carbon Management*, **4**, 591–600.

768   Bartholomé E, Belward a. S (2005) GLC2000: a new approach to global land cover mapping

769   from Earth observation data. *International Journal of Remote Sensing*, **26**, 1959–1977.

770   Bates JM, Granger CWJ (1969) The Combination of Forecasts. *Journal of the Operational*

771   *Research Society*, **20**, 451–468.

772   Birdsey R, Angeles-Perez G, Kurz W a et al. (2013) Approaches to monitoring changes in

773   carbon stocks for REDD+. *Carbon Management*, **4**, 519–537.

774   Breiman L (2001) Random forests. *Machine Learning*, **45**, 5−23.

775   Calders K, Newnham G, Burt A et al. (2015) Nondestructive estimates of above-ground

776   biomass using terrestrial laser scanning. *Methods in Ecology and Evolution*, **6**, 198–208.

777   Cartus O, Kellndorfer J, Walker W, Franco C, Bishop J, Santos L, Michel-Fuentes JM (2014)

778   A National, Detailed Map of Forest Aboveground Carbon Stocks in Mexico. *Remote*

779   *Sensing*, **6**, 5559–5588.

780   Chave J, Olivier J, Bongers F et al. (2008) Above-ground biomass and productivity in a rain

781   forest of eastern South America. *Journal of Tropical Ecology*, **24**, 355–366.

782   DiMiceli CM, Carroll ML, Sohlberg RA et al. (2011) Annual Global Automated MODIS

783   Vegetation Continuous Fields (MOD44B) at 250 m Spatial Resolution for Data Years

784   Beginning Day 65, 2000 - 2010, Collection 5 Percent Tree Cover, University of

785   Maryland, College Park, MD, USA

786   ESA (2014a) Global land cover map for the epoch 2005. http://www.esa-landcover-cci.org/

787   ESA (2014b) Global Water Bodies. http://www.esa-landcover-cci.org/

788   FAO (2000) Global ecological zoning for the global forest resources assessment 2000. FAO

789   FRA Working Paper Rome, Italy; 2001

790   Feldpausch TR, Banin L, Phillips OL et al. (2011) Height-diameter allometry of tropical

791   forest trees. *Biogeosciences*, **8**, 1081–1106.

792   Feldpausch TR, Lloyd J, Lewis SL et al. (2012) Tree height integrated into pantropical forest

793   biomass estimates. *Biogeosciences*, **9**, 3381–3403.

794   Ge Y, Avitabile V, Heuvelink GBM, Wang J, Herold M (2014) Fusion of pan-tropical

795   biomass maps using weighted averaging and regional calibration data. *International*

796   *Journal of Applied Earth Observation and Geoinformation*, **31**, 13–24.

797   Goetz S, Dubayah R (2011) Advances in remote sensing technology and implications for

798   measuring and monitoring forest carbon stocks and change. *Carbon Management*, **2**,

799   231–244.

800   Gonzalez de Tanago J, Bartholomeus H, Joseph S et al. (2015) Terrestrial LiDAR and 3D tree

801   Quantitative Structure Model for quantification of aboveground biomass loss from

802   selective logging in a tropical rainforest of Peru. In: *Proceedings of Silvilaser 2015*

803   *Conference. La Grande Motte, France. 28-30 September 2015*.

804   Grace J, Mitchard E, Gloor E (2014) Perturbations in the carbon budget of the tropics. *Global*

805   *Change Biology*.

806   Harris NL, Brown S, Hagen SC et al. (2012) Baseline Map of Carbon Emissions from

807   Deforestation in Tropical Regions. *Science*, **336**, 1573–1576.

808   Hill TC, Williams M, Bloom A, Mitchard ET, Ryan CM (2013) Are Inventory Based and

809   Remotely Sensed Above-Ground Biomass Estimates Consistent? *PLoS ONE*, **8**, 1–8.

810   Houghton RA, House JI, Pongratz J et al. (2012) Carbon emissions from land use and land-

811   cover change. *Biogeosciences*, **9**, 5125–5142.

812   Jiahui W, Zamar R, Marazzi A, et al. (2014) robust: Robust Library. R package version 0.4-

813   16. http://CRAN.R-project.org/package=robust.

814   Kearsley E, de Haulleville T, Hufkens K et al. (2013) Conventional tree height-diameter

815   relationships significantly overestimate aboveground carbon stocks in the Central Congo

816   Basin. *Nature communications*, **4**, 2269.

817   IPCC (2003) Good practice guidance for land use, land-use change and forestry. IPCC

818   National Greenhouse Gas Inventories Programme, Technical Support Unit. Hayama,

819   Japan: Institute for Global Environmental Strategies.

820   IPCC (2006) 2006 IPCC Guidelines for National Greenhouse Gas Inventories, Prepared by

821   the National Greenhouse Gas Inventories Programme, Eggleston HS, Buendia L, Miwa

822   K, Ngara T and Tanabe K (eds). Published: IGES, Japan.

823   Langner A, Achard F, Grassi G (2014) Can recent pan-tropical biomass maps be used to

824   derive alternative Tier 1 values for reporting REDD+ activities under UNFCCC?

825   *Environmental Research Letters*, **9**, 124008.

826   Lewis SL, Lopez-Gonzalez G, Sonké B et al. (2009) Increasing carbon storage in intact

827   African tropical forests. *Nature*, **457**, 1003–1006.

828   Lewis SL, Sonké B, Sunderland T et al. (2013) Above-ground biomass and structure of 260

829   African tropical forests. *Philosophical transactions of the Royal Society of London.*

830   *Series B, Biological sciences*, **368**, 20120295.

831   Malhi Y, Wood D, Baker TR et al. (2006) The regional variation of aboveground live biomass

832   in old-growth Amazonian forests. *Global Change Biology*, **12**, 1107–1138.

833   Mitchard ET, Saatchi SS, Baccini A, Asner GP, Goetz SJ, Harris NL, Brown S (2013)

834   Uncertainty in the spatial distribution of tropical forest biomass: a comparison of pan-

835   tropical maps. *Carbon balance and management*, **8**, 10.

836   Mitchard ET, Feldpausch TR, Brienen RJW et al. (2014) Markedly divergent estimates of

837   Amazon forest carbon density from ground plots and satellites. *Global Ecology and*

838   *Biogeography*, **23**, 935–946.

839   Nogueira MA, Diaz G, Andrioli W, Falconi FA, Stangarlin JR (2006) Secondary metabolites

840   from Diplodia maydis and Sclerotium rolfsii with antibiotic activity. *Brazilian Journal of*

841   *Microbiology*, **37**, 14–16.

842   Pan Y, Birdsey RA, Fang J et al. (2011) A large and persistent carbon sink in the world's

843   forests. *Science*, **333**, 988–993.

844   Pearson TRH, Brown S, Casarim FM (2014) Carbon emissions from tropical forest

845   degradation caused by logging. *Environmental Research Letters*, **034017**, 11.

846   Phillips O L, Malhi Y, Higuchi N et al. (1998) Changes in the carbon balance of Tropical

847   Forests: Evidence from long-term plots. *Science*, **282**, 439–442.

848   Phillips OL, Aragão LEOC, Lewis SL et al. (2009) Drought sensitivity of the Amazon

849   Rainforest. *Science*, **323**, 1344–1347.

850   Phillips OL, Lewis SL (2014) Evaluating the tropical forest carbon sink. *Global Change*

851   *Biology*, **20**, 2039–2041.

852   Potapov P, Yaroshenko A, Turubanova S et al. (2008) Mapping the world's intact forest

853   landscapes by remote sensing. *Ecology and Society*, **13**.

854   Romijn E, Herold M, Kooistra L, Murdiyarso D, Verchot L (2012) Assessing capacities of

855   non-Annex I countries for national forest monitoring in the context of REDD+.

856   *Environmental Science and Policy*, **19-20**, 33–48.

857   Saatchi SS, Harris NL, Brown S et al. (2011) Benchmark map of forest carbon stocks in

858   tropical regions across three continents. *Proceedings of the National Academy of*

859   *Sciences*, 108, 9899–9904.

860   Saatchi SS, Mascaro J, Xu L et al. (2014) Seeing the forest beyond the trees. *Global Ecology*

861   *& Biogeography*, **23**, 935 – 946.

862   Searle SR (1971) *Linear Models*, Vol. XXI. WILEY-VCH Verlag, York-London-Sydney-

863   Toronto, 532 pp.

864   Simard M, Pinto N, Fisher JB, Baccini A (2011) Mapping forest canopy height globally with

865   spaceborne lidar. Journal of Geophysical Research: Biogeosciences, 116, 1–12.

866 Slik JWF, Aiba SI, Brearley FQ et al. (2010) Environmental correlates of tree biomass, basal

867   area, wood specific gravity and stem density gradients in Borneo's tropical forests.

868   *Global Ecology and Biogeography*, **19**, 50–60.

869 Slik JWF, Paoli G, Mcguire K et al. (2013) Large trees drive forest aboveground biomass

870   variation in moist lowland forests across the tropics. *Global Ecology and Biogeography*,

871   **22**, 1261–1271.

872 Ter Steege H, Pitman NC a, Phillips OL et al. (2006) Continental-scale patterns of canopy

873   tree composition and function across Amazonia. *Nature*, **443**, 444–447.

874 Willcock S, Phillips OL, Platts PJ et al. (2012) Towards Regional, Error-Bounded Landscape

875   Carbon Storage Estimates for Data-Deficient Areas of the World. *PLoS ONE*, **7**, 1–10.

876 Wright JS (2013) The carbon sink in intact tropical forests. *Global Change Biology*, **19**, 337–

877   339.

878 Ziegler AD, Phelps J, Yuen JQ et al. (2012) Carbon outcomes of major land-cover transitions

879   in SE Asia: Great uncertainties and REDD+ policy implications. *Global Change*

880   *Biology*, **18**, 3087–3099.

881 Zolkos SG, Goetz SJ, Dubayah R (2013) A meta-analysis of terrestrial aboveground biomass

882   estimation using lidar remote sensing. *Remote Sensing of Environment*, **128**, 289–298.

883

884

885

886

887

888

889

890

891   **Supporting Information**

892   **Appendix S1**. Supplementary methods and results

893

894

895

896

897

898

899

900

901

902

903

904

905

906

907

908

909

910

911

912   **Tables**

913   **Table 1: Number of reference data (plots and 1-km pixels) selected after the screening, upscaling and**

914   **consolidating procedures, per continent. The reference data selected for each individual dataset are**

915   **reported in Table S1. The field plots underpinning the reference AGB maps are not included.**

Continent	Available	Selected		Consolidated
	Plots	Plots	Pixels	Pixels
Africa	2,281	1,976	953	953
S. America	648	474	449	449
C. America	-	-	5,260	7,675
Asia	3,698	1,833	353	400
Australia	-	-	5,000	5,000
Total	6,627	4,283	12,015	14,477

916

917

918

919

920

921

922

923

924

925

926

927

928   **Figure captions**

929   **Figure 1: Flowchart illustrating the methods for generating the fused biomass map and associated**

930   **uncertainty**

931   **Figure 2: AGB reference dataset for the tropics and spatial coverage of the two input maps**

932   **Figure 3: Fused map, representing the distribution of live woody aboveground biomass (AGB) for all land**

933   **cover types at 1-km resolution for the tropical region.**

934   **Figure 4: Difference maps obtained by subtracting the fused map from the Saatchi map (a) and the**

935   **Baccini map (b).**

936   **Figure 5: RMSE (a) and bias (b) of the fused and input maps per continent obtained using independent**

937   **reference data not used for model development. The error bars indicate one standard deviation of the 100**

938   **simulations. Numbers reported in brackets indicate the number of reference observations used for each**

939   **continent. The results for the pan-tropics exclude Australia, which is not covered by the Baccini map.**
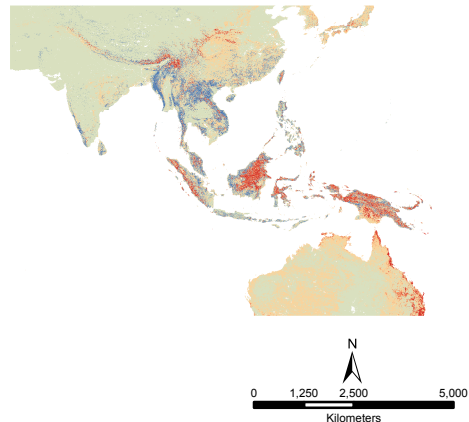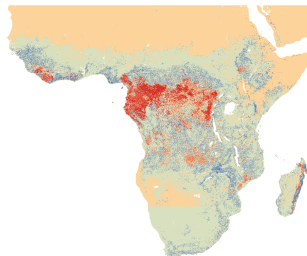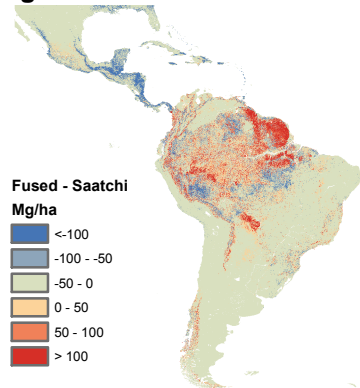
940   **Figure 6: scatterplots of the validation reference data (x-axis) and predictions (y-axis) of the input maps**

941   **(left plots) and fused map (right plots) by continent.**

942   **Figure 7: Uncertainty of the fused map, in absolute values (a) and relative to the AGB estimates (b),**

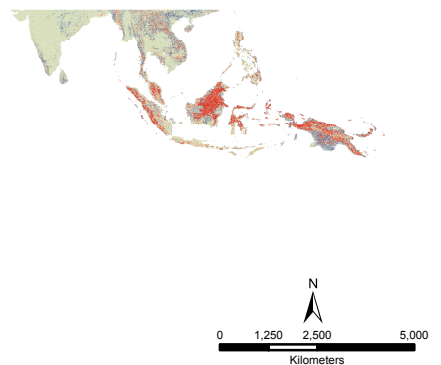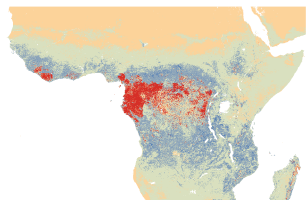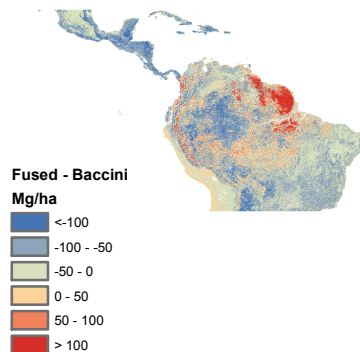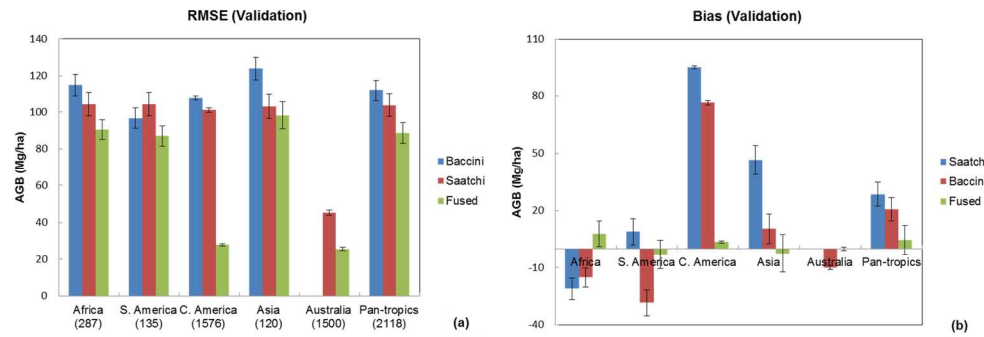943   **representing one standard deviation of the error of the fused map.**

944

945

946

947

948

949

950

951

952

953

954

Reference data
Saatchi extent
Baccini extent

0 1,250 2,500 5,000
Kilometers

AGB (Mg/ha)
- 0
- 0 - 10
- 10 - 25
- 25 - 50
- 50 - 75
- 75 - 100
- 100 - 150
- 150 - 200
- 200 - 300
- 300 - 400
- 400 - 500
- 500 - 620

N

0   1,250   2,500   5,000
Kilometers

(a)

Fused - Saatchi
Mg/ha

- <-100
- -100 - -50
- -50 - 0
- 0 - 50
- 50 - 100
- > 100

N

0   1,250   2,500   5,000
Kilometers

(b)

Fused - Baccini
Mg/ha

- <-100
- -100 - -50
- -50 - 0
- 0 - 50
- 50 - 100
- > 100
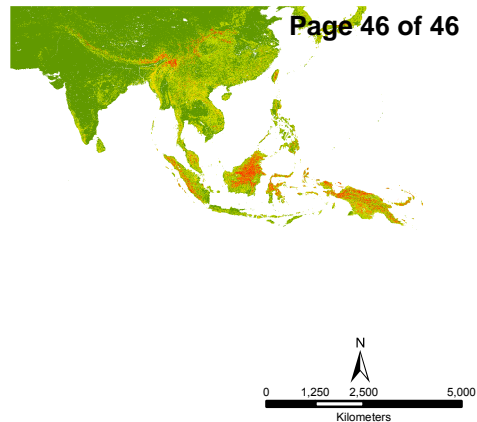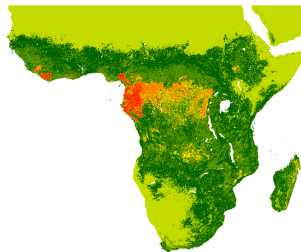
N

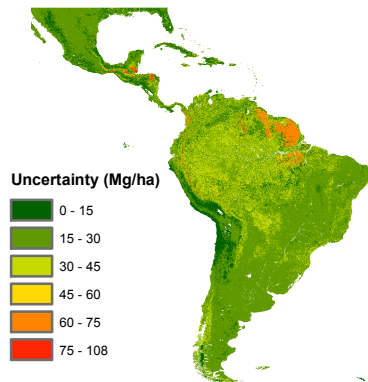0   1,250   2,500   5,000
Kilometers
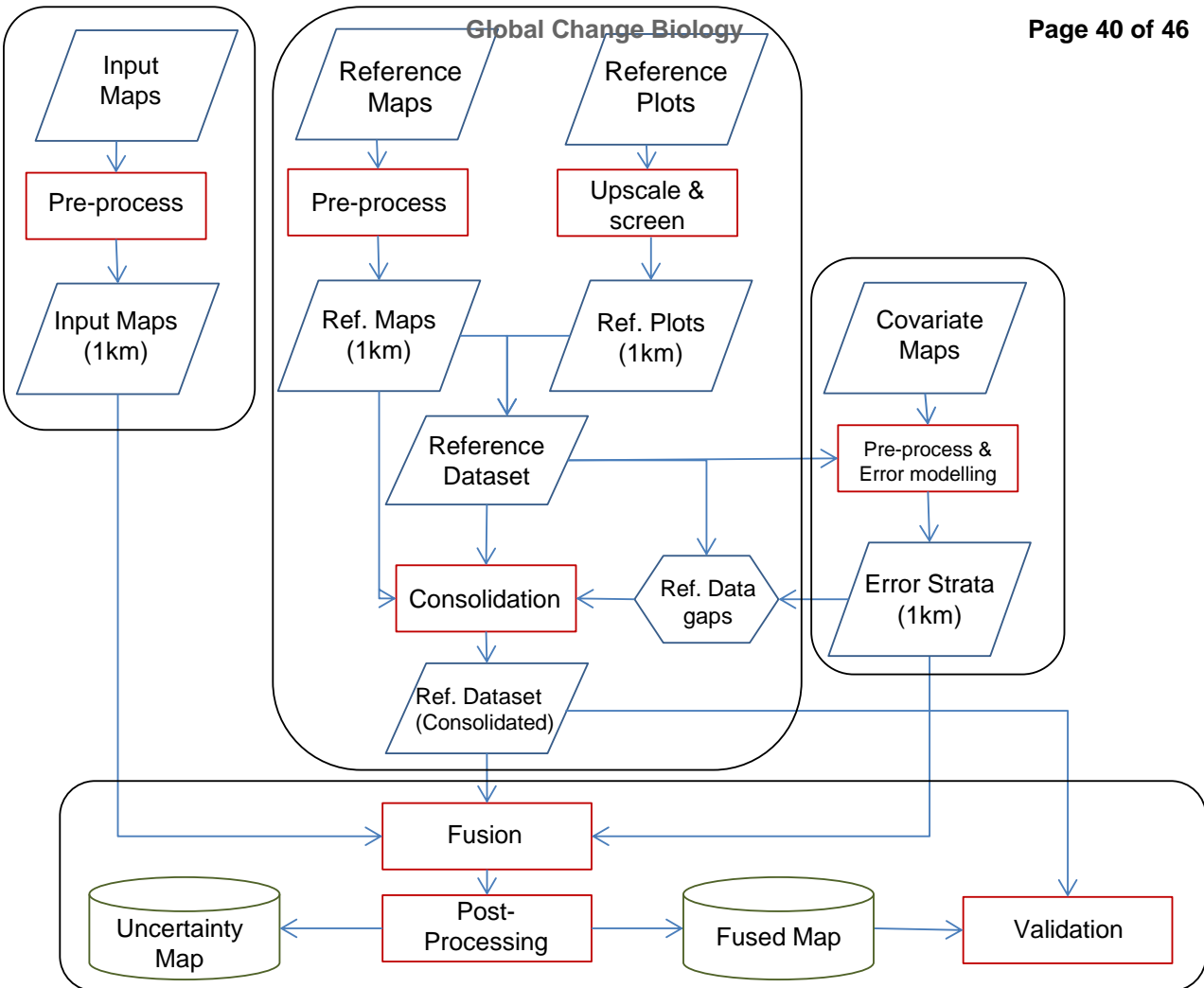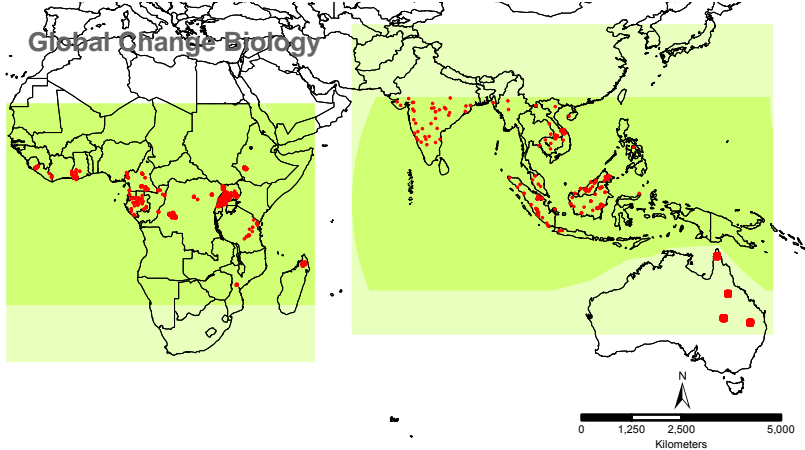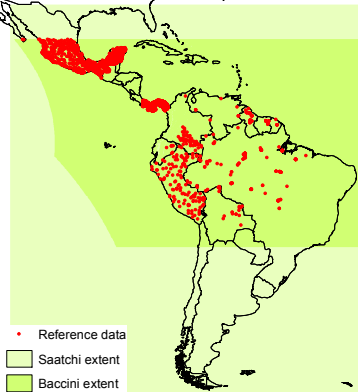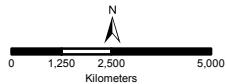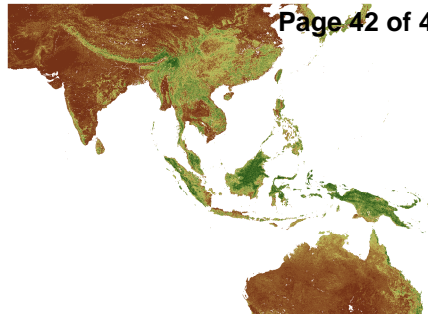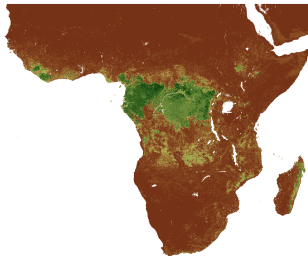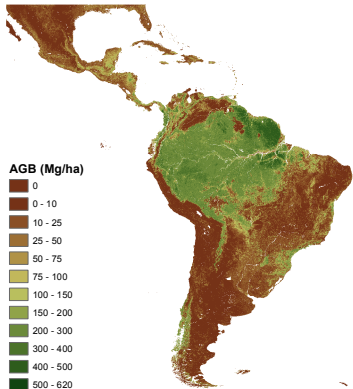
RMSE (a) and bias (b) of the fused and input maps per continent obtained using independent reference data not used for model development. The error bars indicate one standard deviation of the 100 simulations. Numbers reported in brackets indicate the number of reference observations used for each continent. The results for the pan-tropics exclude Australia, which is not covered by the Baccini map.
469x160mm (96 x 96 DPI)
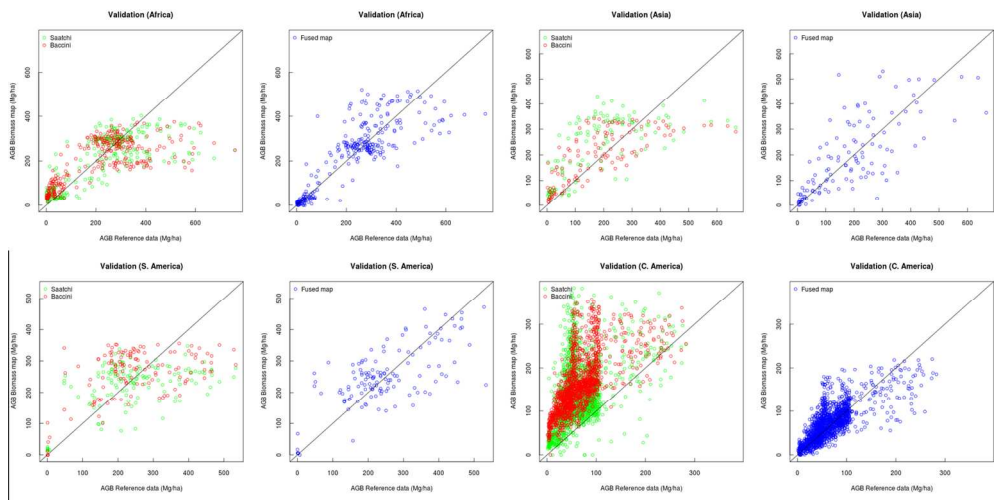
scatterplots of the validation reference data (x-axis) and predictions (y-axis) of the input maps (left plots) and fused map (right plots) by continent.
311x155mm (150 x 150 DPI)

(a)

Uncertainty (Mg/ha)

- 0 - 15
- 15 - 30
- 30 - 45
- 45 - 60
- 60 - 75
- 75 - 108

N

0   1,250   2,500   5,000
Kilometers

(b)

Uncertainty (%)

- 0 - 25%
- 25 - 50%
- 50 - 75%
- 75 - 100%
- > 100%

N

0   1,250   2,500   5,000
Kilometers